Complete spectrum of long-wavelength phonon modes in $Sn_2P_2S_6$ by Raman scattering

J. Hlinka, I. Gregora, and V. Vorlíček
Institute of Physics ASCR, Praha, Czech Republic
(Received 17 September 2001; published 24 January 2002)

The paper presents polarized Raman spectra of $Sn_2P_2S_6$ measured in various backscattering and near-forward and right-angle scattering geometries at $T=15$ K. The complete sets of A'_{TO}, A'_x, A'_z, A''_{TO}, and A''_{LO} mode frequencies are determined. The essential problem of symmetry assignment was solved with the help of measurements of directional dependencies of the oblique mode frequencies.

DOI: 10.1103/PhysRevB.65.064308 PACS number(s): 78.30.−j, 74.25.Kc, 77.80.−e, 63.20.Dj

I. INTRODUCTION

The crystal of $Sn_2P_2S_6$ is a well-known uniaxial semiconductor ferroelectric with Curie point near 337 K.[1,2] Its properties have been recently reinvestigated by a number of methods, including inelastic neutron scattering,[3] x-ray photoemission,[4] birefringence,[5] and Mössbauer[6] and ultrasonic[7] spectroscopies, as well as by dielelectric,[8] acoustoelectric,[9] and electro-optic[10] measurements. Several promising applications of this material have been found, too.[11–16] The basic research on this crystal is also motivated by the lucky occasion that the ambient pressure phase diagram of solid solution $Sn_2P_2S_6$-$Sn_2P_2Se_6$ possesses a so called Lifshitz point, a rare triple point where the paraelectric, ferroelectric, and incommensurate phases simultaneously coincide.[17,18]

There are two equivalent formula units in the monoclinic unit cell of this crystal. In the paraelectric phase ($P2_1/n$, Ref. 19), both symmetrical $Sn_2P_2S_6$ units are located at the center of inversion, which leads to $13B_u+14A_u$ infrared active and $15B_g+15A_g$ Raman active zone center optical modes.[20] In the ferroelectric (Pn) phase[21] the $13B_u+15A_g$ and $14A_u+15B_g$ modes merge into $28A'$ and $29A''$ modes, respectively. The ferroelectric phase transition is continuous, so that just below T_c, A' and A'' modes can be further classified as $A'(A_g)$, $A'(B_u)$, $A''(B_g)$, or $A''(A_u)$. The A' and A'' modes are all simultaneously Raman and infrared active, and they can be, in principle, distinguished by polarization analysis.[20]

The knowledge of the full optic phonon spectrum is obviously quite essential for a design and/or a test of any model of interatomic interactions. Nevertheless, such a full optic phonon spectrum was missing till now. Most of the published Raman data so far were either unpolarized[22] or devoted to the lowest-frequency[23–28] or highest-frequency modes only.[25,28] The full spectral range was covered in Refs. 20 and 29–31, but only Ref. 20 provides a list of observed phonon frequencies. Unfortunately, this early work is based on oblique mode measurements and moreover the reported room temperature spectrum is not quite complete.

Such a situation has probably three essential causes: First, it turns out that the overlap and asymmetry of the phonon lines make any straightforward identification of the observed mode frequencies at $T > 200$ K impossible. Second, the naturally weak (''activated'') $A'(B_u)$ and $A''(A_u)$ modes cannot be easily distinguished from unwanted ''phantoms'' due to an unavoidable polarization leakage or even ''intrinsic disorder'' (reported in Ref. 32). Third, the direction of dipolar strengths of the A' modes is not fixed by symmetry so that one encounters oblique A' modes in almost all usual scattering geometries.

In order to overcome these problems, we have undertaken detailed low-temperature measurements (at about 15 K) in a number of scattering geometries (Fig. 1). As a result, we could determine the complete spectrum of A' and A'' TO modes as well as their dipolar strengths and complicated angular dispersion of the extraordinary (oblique) modes.

II. EXPERIMENTAL DETAILS

The various polished samples used in the present study were cut from single crystals grown by the chemical vapor transfer technique at Uzhgorod University. Crystallographic orientation was determined by optical method in Uzhgorod

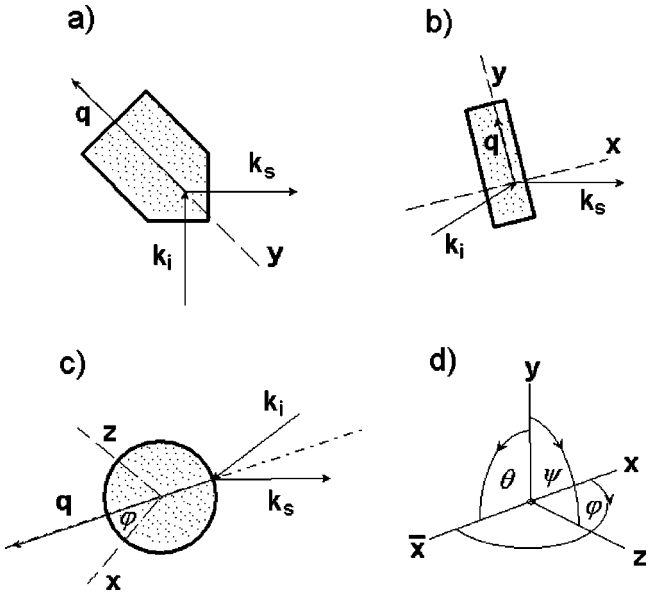

FIG. 1. Scattering geometries used in the present work allows right-angle (a) and near-forward (b) scattering by phonon with wave vector $\mathbf{q}\|\mathbf{y}$, as well as backscattering from cylindrical samples (c) that allows a gradual change of the **q** vector orientation with respect to the crystal axes *x*, *y*, and *z*. The incident and scattered photon wave vectors are denoted $\mathbf{k}_i$ and $\mathbf{k}_s$. Scheme (d) shows angles φ, θ, and ψ used in Figs. 3, 5, and 7.

and checked by x-ray precession photography in our Institute. All the samples were optically transparent, with a typical dark orange color.

Raman scattering experiments were performed with 514.5 nm Ar and 647.1 nm Kr laser excitation lines. The scattered light was analyzed using a SPEX 14018 double spectrometer equipped with standard single-channel photon counting detection. Samples were placed in a continuous-flow liquid-He cryostat, where they were convection cooled in the He exchange gas to about 15 K (as verified from the Stokes to anti-Stokes ratio of the low-frequency spectra). In view of numerous closely separated and overlapping Raman lines, the spectral slit width was kept rather narrow—typically 0.2 cm^{-1} in most of the recorded spectra.

The positions of the lowest-frequency phonons, measured subsequently in Stokes and anti-Stokes spectra, served also for accurate calibration of the origin of the frequency scale (''laser position''). In order to enhance the accuracy further, care was taken to minimize influence of long-term drifts of the spectrometer calibration of the laser and of the strong Raman line (at 384 cm^{-1}) in the course of the measurement cycles. After appropriate calibration corrections, the spectra were reduced, i.e., divided by the Bose-Einstein temperature factor, in order to obtain relative Raman susceptibilities.

Despite the narrow spectral slit width used in our measurements, the peak shapes were often resolution limited. To obtain phonon frequencies, however, the spectra could be satisfactorily fitted to Lorentzian profiles, except in the low-frequency range where fitting by Voigt profiles (Lorenzian convoluted with a Gaussian of appropriate width) gave markedly better results.

Since the aim of the present study was to distinguish among transversal A' and A'' modes as well as various oblique mode frequencies, the polarized Raman spectra were recorded in a number of different scattering geometries (Fig. 1, Table I), allowing to reach the desired combinations of phonon scattering vector **q** and the component of the polarization tensor. To this end we have polished either the flat faces of rectangular samples or surfaces of cylindrical samples having their axes parallel to the crystallographic axes **a** and **b**.

Here and further on, **x**,**y**,**z** are parallel to the **a**,**b**,**c** edges of the ''pseudo-orthorhombic'' unit cell with $\beta = 91.5°$, and $a > b > c$. For the purposes of this paper, the difference between 91.5° and 90° can be neglected and the directions **x** and **z** are regarded as perpendicular. Then, the Raman tensor components (xy) and (yz) correspond to A'', while (xz) and all diagonal components correspond to the A' irreducible representation.[29] It can be seen from the Table I that the A'_{TO} and A''_{TO}, as well as the oblique modes A'_x and A'_z (with $\mathbf{q}\|\mathbf{x},\mathbf{q}\|\mathbf{z}$) can be measured in the standard backscattering geometry. Unfortunately, scattering by the A''_{LO} modes cannot be realized in any backscattering geometry. For this reason, the two unconventional right-angle [Fig. 1(a)] and near-forward [Fig. 1(b)] scattering geometries were devised, allowing observation of A''_{LO} modes. The angle between incident and scattered photon wave vectors in near-forward scattering was as large as 12° (outside of the sample), in order to avoid polariton effects.

TABLE I. Various geometrical arrangements for Raman scattering used in the present study. The labels *b* corner, *a* plate, and *b* cylinder in the second column refer to the scattering geometries sketched in Figs. 1(a), 1(b), and 1(c) respectively, and horizontal (H) and vertical (V) polarization is defined with respect to the horizontal scattering plane defined by $\mathbf{k}_i$ and $\mathbf{k}_s$ wave vectors in Figs. 1(a)–1(c).

Scattering mode	Type of sample		Selected phonons	Polarization
Back	*a* face	$\mathbf{q}\|\mathbf{x}$	A''_{TO} A'_x	$x(zy)\bar{x}$ $x(yy)\bar{x}, x(zz)\bar{x}$
Back	*b* face	$\mathbf{q}\|\mathbf{y}$	A'_{TO}	$y(zx)\bar{y}, y(xx)\bar{y}$, $y(zz)\bar{y}$
Back	*c* face	$\mathbf{q}\|\mathbf{z}$	A''_{TO} A'_z	$z(xy)\bar{z}$ $z(yy)\bar{z}, z(xx)\bar{z}$
Right angle	*b* corner	$\mathbf{q}\|\mathbf{y}$	A'_{TO} A'_{TO}, A''_{LO}	VV HV
Forward	*a* plate	$\mathbf{q}\|\mathbf{y}$	A''_{LO} A'_{TO}	$x(zy)x$ $x(yy)x$
Back	*b* cylinder	$\mathbf{q}\perp\mathbf{y}$	A', A''_{TO}	Unpolarized
Back	*a* cylinder	$\mathbf{q}\perp\mathbf{x}$	A	VH

Finally, the cylindrical samples [Fig. 1(c)] allowed to investigate angular dispersion curves of oblique modes by means of systematic backscattering measurements at various angles of incidence (each 10°). Due to a small (5 mm) cylinder diameter, we have probably introduced an error of $\pm 3°$ in each angle setting, but this error did not accumulate since the crystal holder was fixed directly to the goniometric circle. Actually, such random angular fluctuations turned out to be negligible here because of the relatively mild and smooth course of the observed angular dispersion.

III. SYMMETRY ASSIGNMENT OF THE OBSERVED RAMAN LINES

One can consider the $Sn_2P_2S_6$ crystal as consisting of Sn^{2+} cations and $P_2S_6^{4-}$ molecular anions.[33–35] Let us first imagine $P_2S_6^{4-}$ anions to be relatively rigid, so that the interaction between the mentioned constituents are negligible in comparison with intramolecular forces. The vibrational spectrum should in this case split into two distinct parts—a high-frequency part involving internal degrees of freedom of the $P_2S_6^{4-}$ anion and a low-frequency part including the external modes (translations of Sn^{2+} and $P_2S_6^{4-}$ and $P_2S_6^{4-}$ rotations). In the case of the ferroelectric phase, one would expect 10 A' and 11 A'' external modes and 18 Davydov doublets (A',A'') of internal modes.

In reality, the concept of $P_2S_6^{4-}$ anions has somewhat limited applicability here. The theoretical estimations[35] show

TABLE II. Frequencies of A' Raman modes at 15 K. Frequencies $\Omega_\mu[\hat{\mathbf{x}}]$ and $\Omega_\mu[\hat{\mathbf{z}}]$ correspond to the μth oblique modes with wave vectors $\mathbf{q}\|\hat{\mathbf{x}}$ and $\mathbf{q}\|\hat{\mathbf{z}}$, respectively, while φ_μ and $|S_\mu|$ give the orientation and absolute value of the screened dipolar strength vector $\mathbf{S}_\mu$ defined by Eq. (7) in Sec. IV.

μ	Ω_μ[TO] (cm^{-1})	$\Omega_\mu[\hat{\mathbf{x}}]$ (cm^{-1})	$\Omega_\mu[\hat{\mathbf{z}}]$ (cm^{-1})	$\lvert S_\mu\rvert$ (cm^{-1})	φ_μ (deg)
1	589.85	600.90	594.70	108	22
2	581.45	581.90	586.30	76	113
3	569.65	569.90	573.40	74	103
4	559.90	562.60	560.00	56	5
5	556.40	557.15	559.50	87	120
6	442.95	445.20	443.75	51	31
7	384.05	384.05	384.25	12	77
8	275.15	279.00	281.95	58	56
9	269.45	269.50	269.60	11	67
10	250.00	259.65	250.30	59	8
11	247.65	248.05	248.00	31	19
12	215.85	216.20	231.00	68	82
13	206.25	210.05	206.50	39	19
14	196.75	196.75	198.40	27	94
15	181.85	182.45	183.25	21	61
16	177.35	178.65	178.40	26	133
17	166.05	166.95	168.60	29	65
18	145.65	150.25	146.00	9	35
19	128.20	144.65	141.30	21	102
20	121.55	128.15	126.60	37	124
21	106.90	120.75	116.15	83	1
22	94.45	98.20	106.90	47	17
23	82.80	89.25	94.20	69	16
24	79.60	80.15	82.70	113	107
25	70.10	72.20	70.83	53	36
26	59.55	60.15	59.70	22	157
27	46.05	46.30	51.80	45	103
28	39.10	39.35	41.90	47	101

TABLE III. Frequencies of A'' Raman modes at 15 K.

μ	Ω_μ[TO] (cm^{-1})	Ω_μ[LO] (cm^{-1})	$\lvert S_\mu\rvert$ (cm^{-1})
1	601.80	607.1	65
2	586.45	587.7	31
3	571.90	578.5	90
4	563.75	564	21
5	558.90	560	46
6	440.25	441	25
7	381.95	382.1	10
8	284.20	289	9
9	278.50	284	65
10	264.05	266	38
11	251.00	251.3	14
12	227.55	228	14
13	218.15	218.5	12
14	208.50	209	13
15	202.60	203	12
16	189.85	191	18
17	183.55	184	12
18	160.50	160.7	5
19	152.50	154.4	14
20	138.70	144	21
21	132.05	133.7	13
22	119.70	125.2	4
23	107.30	119.5	9
24	87.95	107	54
25	78.35	85	74
26	73.60	74.7	42
27	61.05	61.9	3
28	56.50	61	57
29	41.10	42.4	25

that the lowest-frequency vibrational frequencies of a free $P_2S_6^{4-}$ anion (such as the twist of PS_3 groups around the P-P bond) are comparable with the frequencies of the external modes. The experimental spectrum does not show any clear gap between internal and external modes either. Nevertheless, the seven bond stretching modes ($E_u+E_g+A_{2u}+2A_g$, corresponding to six P-S and one P-P essentially covalent bonds of $P_2S_6^{4-}$) are well separated from the rest of the spectrum. In the $Sn_2P_2S_6$ crystal, they give rise to seven Davydov doublets (A',A''). Five of them belong to the 550–610 cm^{-1} band, while the remaining two doublets are located near 384 cm^{-1} and 440 cm^{-1} in $Sn_2P_2S_6$ crystal itself[20,22] as well in a number of other crystals containing $P_2S_6^{4-}$ units.[30,36–38]

Systematic assignment of the internal modes below 300 cm^{-1} on the basis of the available model calculations for the isolated $P_2S_6^{4-}$ ion is still problematic, and although it was proposed by several authors[22,20,30] in the past, we will not try to do it here. Instead, we concentrate on the classification of the observed modes by relevant irreducible representations (A',A''), and on phonon wave vector (taking care to distinguish frequencies of TO, LO, and oblique modes). The results are given in Tables II and III. Since this task for the $Sn_2P_2S_6$ crystal is completely solved, we describe the procedure in detail below.

A. 550–610 cm^{-1} band

As just mentioned, there are five A' and five A'' modes expected in this frequency band. All five A'_{TO} frequencies can be indeed found from our $y(xx)\bar{y}$ spectra in agreement with previous studies (Fig. 2). Figure 3(a) shows the angular dependence of the frequency of the modes with $\mathbf{q}\perp\mathbf{y}$. The angle between $\mathbf{q}$ and $\mathbf{x}$ in the $\mathbf{xz}$ plane denoted φ ranges only from 0 to π, because the π–2π interval is equivalent [see Fig. 1(d)]. The data represented by full circles in Fig. 3(a) were obtained from the measurements in backscattering geometry without a polarizer, so that both A' and A'' modes do contribute simultaneously. However, they are easy to distinguish. The five branches with no angular dependence correspond to the A''_{TO} frequencies, because the scattering phonon

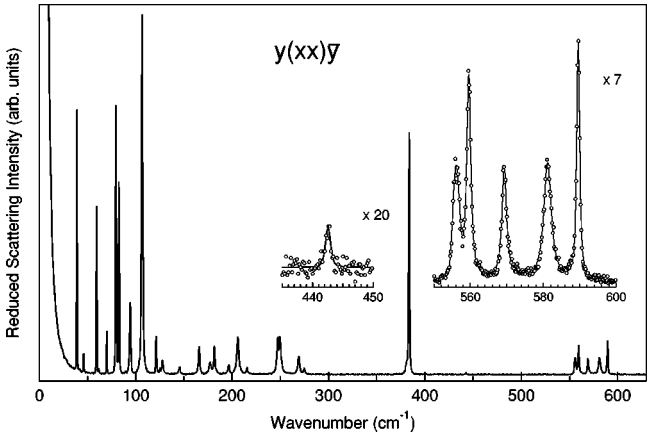

FIG. 2. Raman spectrum in the $y(xx)\bar{y}$ scattering geometry at $T=15$ K. Insets: Enlarged spectra of high-frequency A'_{TO} stretching modes.

wave vector **q** remains perpendicular to the dipole moment associated with the A'' modes. On the other hand, dipolar moments of the A' modes lie in the **xz** plane so that the macroscopic depolarization field causes the observed angular dispersion of the five A' branches.

With the help of the Fig. 3(a) we could safely assign all the modes in the standard backscattering spectra, including the ''ghosts'' due to the polarization leakage. The spectra were then fitted by an appropriate number of Lorentzian peaks in order to obtain the A''_{TO}, A'_x and A'_z frequencies provided in the Tables II and III. Let us stress that the step of mode assignment based on the continuity of angular dispersion in Fig. 3(a) was a very essential one. For example, we would otherwise hardly know that the strongest peak in the $z(yy)\bar{z}$ spectra (see bottom of Fig. 4) is actually a A'-A' doublet. Figure 4 shows that this doublet becomes clearly distinguished at another angle of incidence. Additionally, recording the whole angular dependence allows us to ''tune'' the optimal geometry for the modes with very weak intensity. For example, without Fig. 3(a) we would completely miss the A'_z mode near 586.3 cm^{-1}, which has very low intensity in both $z(xx)\bar{z}$ and $z(yy)\bar{z}$ spectra.

Figure 3(c) shows the angular dispersion in the **yz** plane. The angle ψ between **q** and **y** is taken between 0 and $\pi/2$ only since the rest is merely related by symmetry. As the wave vector of the phonon involved in scattering is now in a general position with respect to the symmetry plane, the A' and A'' modes are mutually coupled. The observed branches are of a mixed A'–A'' character and the exact A' and A'' symmetry is recovered only for $\mathbf{q}\|\mathbf{y}$ and $\mathbf{q}\|\mathbf{z}$. The dispersion curves were obtained in backscattering geometry with crossed polarizations (in order to favor the A''-like modes.) One of the polarizations was kept parallel to **x** direction so that the $\mathbf{q}\|\mathbf{z}$ measurement corresponded to the $z(yx)\bar{z}$ geometry, which allows A''_{TO} modes. Actually, some of the A'_z modes were observed due to the polarization leakage, too. The $\mathbf{q}\|\mathbf{y}$ limit case represents the $y(zx)\bar{y}$ geometry. No extra modes due to the polarization leakage are expected

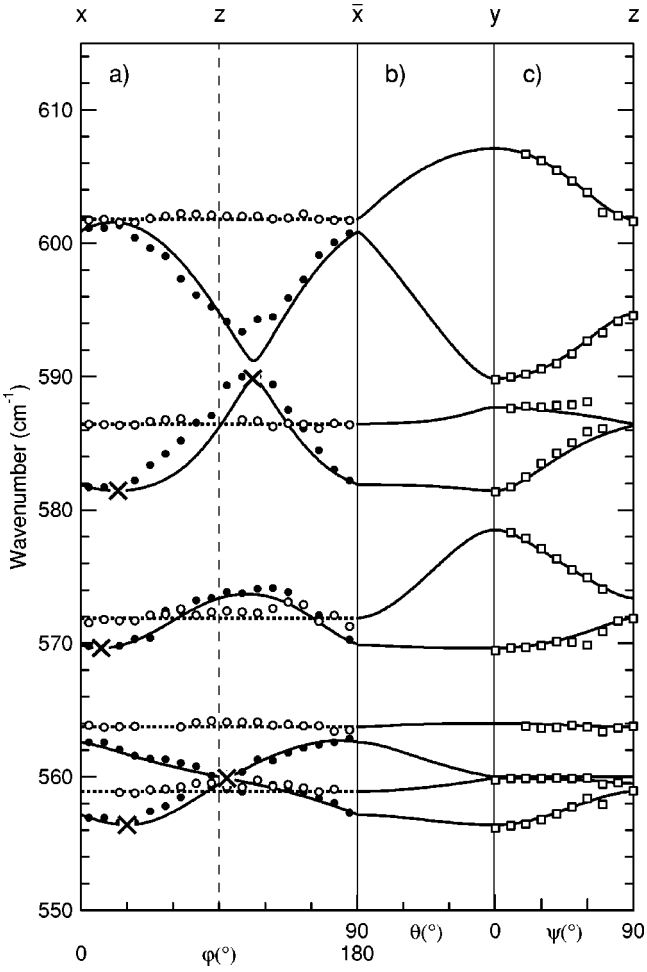

FIG. 3. High-frequency stretching mode frequencies as a function of phonon wave vector direction. Parts (a), (b), and (c) shows dependence on angle φ with $\mathbf{q}\perp\mathbf{y}$, angle θ with $\mathbf{q}\perp\mathbf{z}$ and angle ψ with $\mathbf{q}\perp\mathbf{x}$, respectively [see Fig. 1(d)]. Small symbols are experimental phonon frequencies and full and open circles stand for the modes assigned as A'_1–A'_5 and A''_1–A''_5 modes, respectively. The continuous curves are calculated according to the procedure described in Sec. IV and large crosses (×) mark their maxima or minima associated with independently determined TO frequencies.

here—both $y(xx)\bar{y}$ and $y(zz)\bar{y}$ would provide A' modes. As already mentioned, the A'' modes with $\mathbf{q}\|\mathbf{y}$ (A''_{LO} modes) cannot be detected in an ideal backscattering geometry at all. Nevertheless, the missing values of A''_{LO} frequencies can be obtained by extrapolating of the A'–A'' mixed branches in Fig. 3(c) to the $\mathbf{q}\|\mathbf{y}$ limit. Obviously, the required A''_{LO} frequencies are those that do not coincide with the previously determined A'_{TO} frequencies. Four of the five searched A''_{LO} frequencies are determined without ambiguity; the remaining A''_{LO} mode is partly overlapped by a nearby A'_{TO} mode. Thus, we can only say that its frequency is around 560 cm^{-1}.

B. 440 and 384 cm^{-1} bands

Assignment of the two Davydov pairs near 440 and 384 cm^{-1} is quite easy since both bands are well separated from other parts of the frequency spectrum. The 440 cm^{-1}

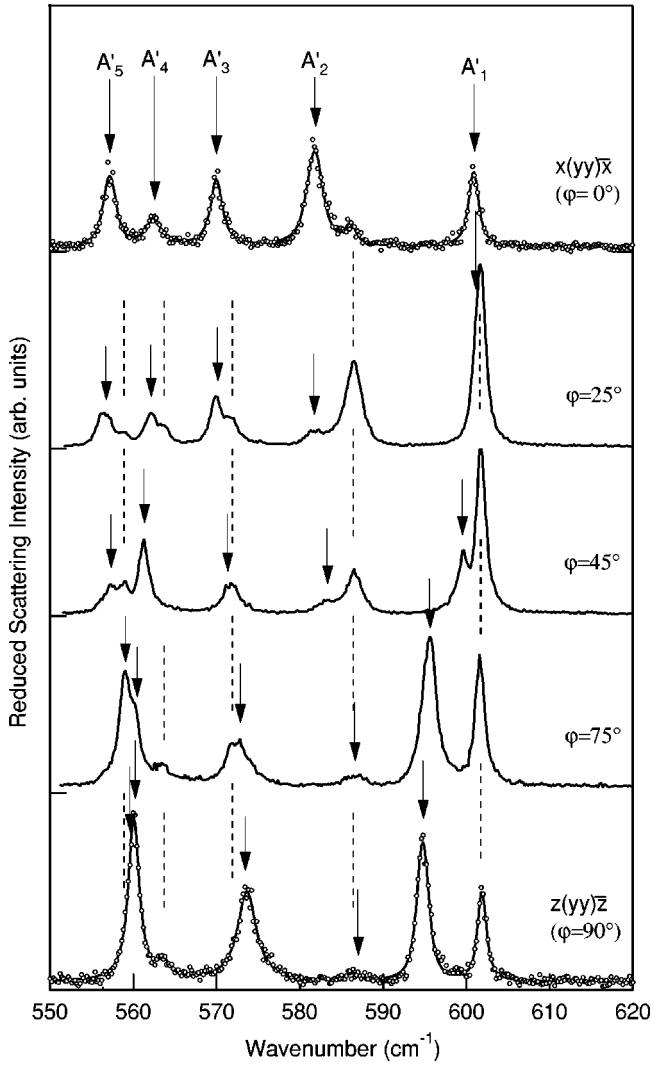

FIG. 4. Backscattering Raman spectra for different phonon wave vector orientations. Dashed lines correspond to the position of dispersionless A'' modes, arrows to the oblique A' modes. Top and bottom spectra are polarized (yy); spectra taken for intermediate angles are not polarized.

band, originating from the A_{2u} band of P_2S_6, is necessarily of a very low scattering intensity (enlarged in inset of Fig. 2). In spite of that we were able to distinguish $A'_{TO}=443\ cm^{-1}$, $A''_{TO}=440.3\ cm^{-1}$, $A'_x=445.2\ cm^{-1}$, and $A'_z=443.7\ cm^{-1}$. We have no clear direct observation of A''_{LO}, but it seems that the assumption $A''_{LO}-A''_{TO}\leqslant 1\ cm^{-1}$ is quite consistent with our data and calculations[35] as well as published ir spectra.[22]

On the other hand, the 384 cm^{-1} line is one of the strongest Raman lines in the whole spectrum. In all our spectra we have actually observed a doublet which we interpret as due to the Davydov $(A'-A'')$ splitting. Using suitable backscattering geometries we have obtained $A'_{TO}=384.05\ cm^{-1}$, $A'_x=384.05\ cm^{-1}$, $A'_z=384.25\ cm^{-1}$, and $A''_{TO}=382\ cm^{-1}$. The remaining frequency $A''_{LO}=382.1\ cm^{-1}$ was obtained from the near-forward scattering geometry.

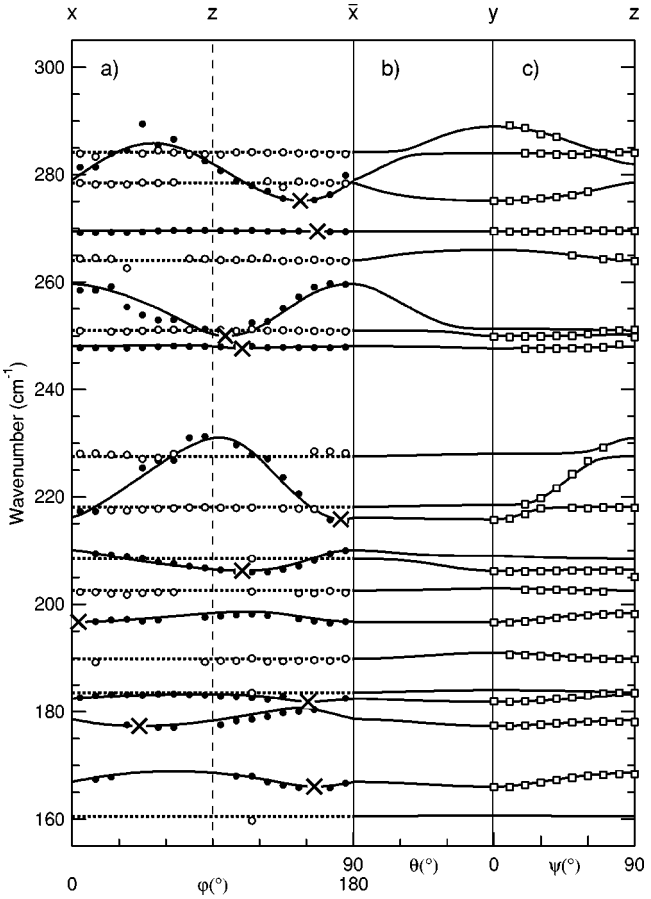

FIG. 5. Angular dispersion in the 150–300 cm^{-1} region. Parts (a), (b), and (c) show the dependence on angle φ with $\mathbf{q}\perp\mathbf{y}$, angle θ with $\mathbf{q}\perp\mathbf{z}$, and angle ψ with $\mathbf{q}\perp\mathbf{x}$, respectively, as in Fig. 3.

C. 240–300 cm^{-1} band

There is a kind of gap around 240 cm^{-1} in all the measured spectra, so that it is convenient to consider the 240–300 cm^{-1} band separately. In total, eight branches were found on the $\mathbf{q}\perp\mathbf{y}$ angular dispersion in this frequency region. Half of them were attributed to the A' modes [two of them due to the obvious dispersion (see Fig. 5)], and two flat ones due to the correspondence with independent measurement of A'_{TO} modes in $y(xz)\bar{y}$, $y(zz)\bar{y}$, and $y(xx)\bar{y}$ geometry (last given in Fig. 2).

The A''_{TO} frequencies were obtained by extrapolation of the **y**-**z** angular dispersion as in Sec. III A, except for the lowest-frequency A'' mode. Its frequency was obtained directly from one of our $y(xx)\bar{y}$ spectra where this mode appeared as a clear shoulder. (A mode with **q** not exactly parallel to **y** could contribute due to a finite aperture of the detector or small missalignment.)

D. Modes below 240 cm^{-1}

Quite similarly, one can assign the remaining 17 A' and 18 A'' modes below 240 cm^{-1}. These obvious rules were useful in the identification of A'-type modes:

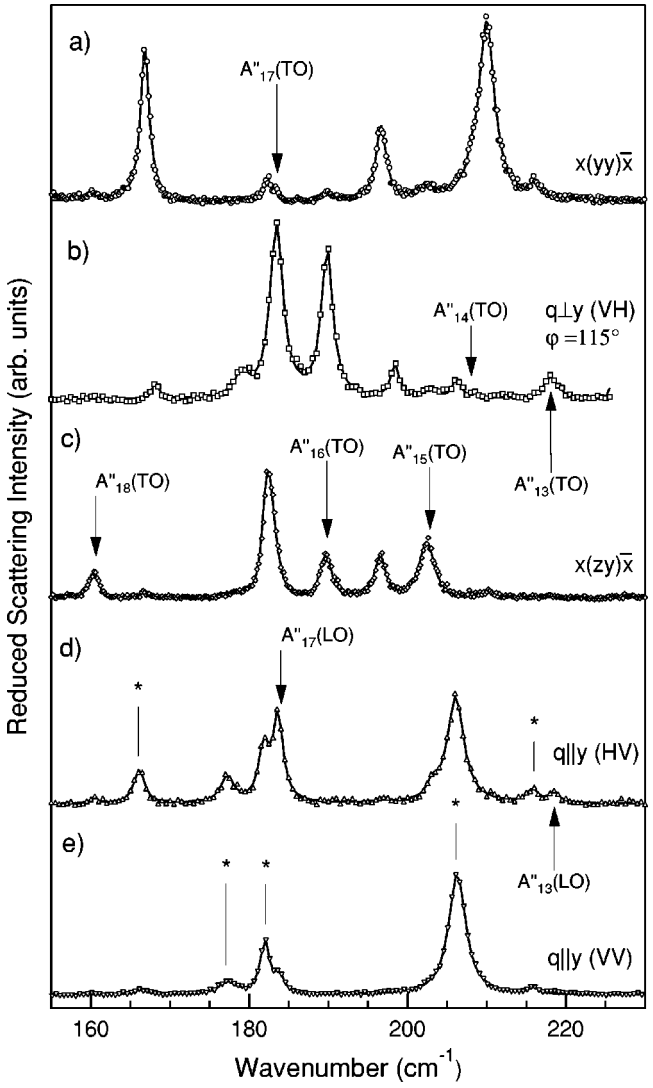

FIG. 6. Observations of the A'' modes in various scattering geometries. Point symbols are experimental data; solid lines show fitting by a sum of Lorentzian curves. The upper mode from the doublet near 180 cm^{-1} in the backscattering $x(yy)\bar{x}$ spectrum (a) could be assigned as the A'' mode because it appeared as quite a strong peak in VH polarized spectra for certain directions of phonon wave vector $\mathbf{q}\perp\mathbf{y}$ (b). The $\mathbf{x}(\mathbf{zy})\bar{\mathbf{x}}$ spectrum (c) allows us to identify the A''_{18} (TO) mode, which is missing in almost all other spectra. The relative intensity contrast between HV (d) and VV (e) polarized right-angle scattering spectra allows us to identify A''(LO) modes, such as A''_{17}(LO).

(1) Branches with clear dispersion in the xz plane belong to the A' type.

(2) There is just a single A'-type branch in between of the two subsequent A'_{TO} frequencies.

(3) Every A'_{TO} corresponds to a pair of inversion related extrema of an A'-type branch.

Let us comment only on the few A'' modes that deserve particular caution. At first, there are two A''_{TO} modes that are almost completely masked by the neighboring A' modes: the A''_{TO} modes near 183 and 208 cm^{-1}. The 183 cm^{-1} doublet was partially resolved in our $x(zz)\bar{x}$ and $x(yy)\bar{x}$ spectra [the latter shown in Fig. 6(a)]. As the higher peak of the doublet corresponds to the maximum found in the cross-polarized geometry with one polarizer along the $\hat{\mathbf{y}}$ direction [backscattering with $\mathbf{q}\perp\hat{\mathbf{y}}$, $\varphi=115°$, shown in Fig. 6(b)], we have assigned the higher peak as an A'' mode. The A''_{TO} mode appeared near 208 cm^{-1} as a shoulder of the 13th A' branch in a number of spectra, but it could be resolved only in cross-polarized spectra for $\varphi=115°$ [Fig. 6(b)]. Second, there is a very weak A''_{TO} mode near 160 cm^{-1}, which was clearly seen only in $x(zy)\bar{x}$ spectrum [Fig. 6(c)]. Finally, due to the mode overlapping or small intensity, we could determine only a few A''_{LO} modes from the $\mathbf{q}\perp\mathbf{x}$ angular dispersion. For this reason, two complementary scattering geometries allowing measurement of $\mathbf{q}\|\mathbf{y}$ modes were used to record complementary information. For example, the A''_{LO} near 183 cm^{-1} was detected in right-angle geometry [compare cross-polarized HV and parallel-polarized VV spectra in Figs. 6(d) and 6(e)] while the A''_{LO} modes near 209 and 228 cm^{-1} were found in near-forward scattering.

E. Synthesis and general remarks

In total, we have analyzed about 100 different spectra. All observed features have been consistently assigned by the method described above. As a result, we have observed Raman lines corresponding to all 28 A' and 29 A'' TO modes and a vast majority of the searched oblique modes. We could also determine all 29 A''_{LO} frequencies, although resolution of three of them (228, 441, and 561 cm^{-1}) was quite difficult so that these three frequencies are determined with a larger error of about ± 2 cm^{-1}.

After completing the mode assignment, several spectral measurements were repeated in order to test the experimental error in frequency determinations. It turned out that the reproducibility was excellent (± 0.3 cm^{-1}), but since the analysis showed that these frequency shifts are quite systematic and smoothly evolving with the measurement time (0.1 cm^{-1}/h), additional corrections were made. For this purpose, the average measured frequency of the strong 384.05 cm^{-1} A'_{TO} mode was taken as a reference, and the frequency scale of all spectra was contracted or elongated in order to match the reference mode frequency exactly. Such a correction, applied to the data in the Tables II and III, never exceeds 0.3 cm^{-1}, but it clearly leads to smoothing of the angular phonon dispersions (Figs. 3, 5, and 7). This shows that the corrected *relative* phonon frequency precision of well-resolved peaks is actually better than 0.1 cm^{-1}. Obviously, the absolute precision of the frequencies in Table II is only about 1 cm^{-1}.

IV. DIPOLAR STRENGTHS AND DISPERSION OF OBLIQUE MODES

Due to the lack of an inversion center in the investigated crystal, all the optic modes are polar. Therefore, each phonon coordinate can be associated with a dipolar moment $\mathbf{d}_\mu = e^*_\mu \mathbf{u}_\mu$, where e^*_μ and $\mathbf{u}_\mu = |\mathbf{u}_\mu|\hat{\mathbf{u}}_\mu$ are the conveniently chosen effective charge and amplitude of displacement of the

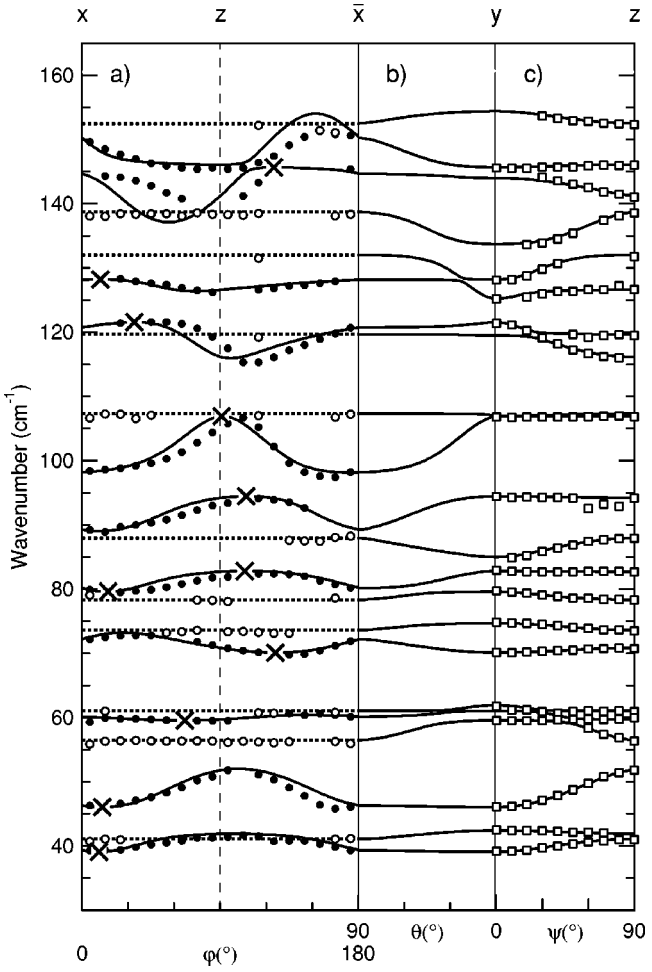

FIG. 7. Angular dispersion in the 30–150 cm^{-1} region. Parts (a), (b), and (c) show the dependence on angles φ, θ, and ψ, respectively, as in Figs. 3 and 5.

μth mode (such that $e_\mu^* \mathbf{u}_\mu$ gives the dipole moment of the unit cell). For a μth mode with a small but finite wave vector $\mathbf{q}$, displacement of the μth phonon coordinate creates a depolarization field[39,40] with amplitude

$$\mathbf{E}_{\mathrm{dep},\mu}[\hat{\mathbf{q}}] = -\frac{e_\mu^*}{\epsilon_0 V_0}(\mathbf{u}_\mu \cdot \hat{\mathbf{q}})\hat{\mathbf{q}}, \tag{1}$$

where $\hat{\mathbf{q}} = \mathbf{q}/q$ is the unit vector parallel to the phonon wave vector and V_0 is the unit cell volume. We have seen that by a convenient choice of the phonon wave vector, the depolarization field can be completely eliminated either for all A' modes (if $\hat{\mathbf{q}} \| \mathbf{y}$) or for all A'' modes (if $\hat{\mathbf{q}} \perp \mathbf{y}$). Let us now consider the general case when the depolarization field is nonzero, i.e., $\hat{\mathbf{q}} \cdot \mathbf{u}_\mu \neq 0$. The harmonic equation of motion for such a mode can be written as

$$m_\mu \ddot{\mathbf{u}}_\mu + m_\mu \Omega_\mu^2[\mathrm{TO}]\mathbf{u}_\mu = e_\mu^*(\mathbf{E}_{\mathrm{dep}}[\hat{\mathbf{q}}] \cdot \hat{\mathbf{u}}_\mu)\hat{\mathbf{u}}_\mu, \tag{2}$$

where m_μ and $\Omega_\mu^2[\mathrm{TO}]$ are the effective mass and the square of the transversal optic frequency associated with $\mathbf{u}_\mu$, respectively. The total depolarization field $\mathbf{E}_{\mathrm{dep}}[\hat{\mathbf{q}}]$ includes contributions of all the modes with $\hat{\mathbf{q}} \cdot \mathbf{u}_\nu \neq 0$:

$$\mathbf{E}_{\mathrm{dep}}[\hat{\mathbf{q}}] = \chi_\infty \cdot \mathbf{E}_{\mathrm{dep}}[\hat{\mathbf{q}}] - \sum_\nu \frac{e_\nu^*}{\epsilon_0 V_0}(\mathbf{u}_\nu \cdot \hat{\mathbf{q}})\hat{\mathbf{q}}, \tag{3}$$

where χ_∞ is the high-frequency susceptibility tensor.

Combining Eqs. (2) and (3) provides a homogeneous set of bilinearly coupled equations of motion. The dynamical matrix of such system, written in the basis of TO modes, reads simply:[42]

$$(D)_{\mu,\nu} = \delta_{\mu,\nu}\Omega_\mu^2[\mathrm{TO}] + \frac{1}{\epsilon(\hat{\mathbf{q}},\infty)}(\mathbf{M}_\nu \cdot \hat{\mathbf{q}}) \cdot (\mathbf{M}_\mu \cdot \hat{\mathbf{q}}), \tag{4}$$

where the angular function

$$\epsilon(\hat{\mathbf{q}},\infty) = 1 + \hat{\mathbf{q}} \cdot \chi_\infty \cdot \hat{\mathbf{q}} \tag{5}$$

(given in a somewhat less general form in Ref. 42) describes the screening by the high-frequency dielectric response appropriate for a field along $\hat{\mathbf{q}}$ and

$$\mathbf{M}_\mu = \frac{e_\mu^* \hat{\mathbf{u}}_\mu}{\sqrt{m_\mu \epsilon_0 V_0}} \tag{6}$$

are the usual vectorial dipolar strengths.[42]

The frequencies of the oblique (extraordinary) modes for any $\hat{\mathbf{q}}$ can be obtained as square roots of eigenvalues of the above dynamical matrix [Eq. (4)]. Obviously, $M_{\mu,x} = M_{\mu,z} = 0$ for all A'' modes and $M_{\mu,y} = 0$ for all A' modes. Moreover, the $(\mathbf{M}_\nu \cdot \hat{\mathbf{q}}) \cdot (\mathbf{M}_\mu \cdot \hat{\mathbf{q}})/\epsilon(\hat{\mathbf{q}},\infty)$ in the dynamical matrix [Eq. (4)] can be well approximated by $(\mathbf{S}_\nu \cdot \hat{\mathbf{q}}) \cdot (\mathbf{S}_\mu \cdot \hat{\mathbf{q}})$ with screened dipolar strengths

$$\mathbf{S}_\mu = \frac{\mathbf{M}_\mu}{\sqrt{\epsilon(\hat{\mathbf{u}}_\mu,\infty)}}, \tag{7}$$

since the high-frequency dielectric constant measured along the principal directions differs[43] by less than 10% in our case. Consequently, we can use approximative dynamical matrix

$$(D)_{\mu,\nu} = \delta_{\mu,\nu}\Omega_\mu^2[\mathrm{TO}] + (\mathbf{S}_\nu \cdot \hat{\mathbf{q}}) \cdot (\mathbf{S}_\mu \cdot \hat{\mathbf{q}}), \tag{8}$$

which is equivalent to the one introduced in Refs. 39 and 40; for its definition only the complete sets of $\Omega_\mu^2[\mathrm{TO}]$ and $\mathbf{S}_\mu$ are necessary.

These parameters can be found by fitting the measured dispersion curves, as suggested e.g., in Ref. 40. However, since the exact analytical solution for the present inverse eigenvalue problem is known, one can evaluate the absolute values of Cartesian components $S_{\mu i}$ directly using the phonon frequencies from Tables II and III. Applying the well-known relations[41] subsequently to A''_{LO} mode frequencies $\Omega_\nu[\mathrm{LO}]$,

$$|S_{\mu y}| = \sqrt{\frac{\Pi_\nu(\Omega_\nu^2[\mathrm{LO}] - \Omega_\mu^2[\mathrm{TO}])}{\Pi_{\nu\neq\mu}(\Omega_\nu^2[\mathrm{TO}] - \Omega_\mu^2[\mathrm{TO}])}}, \tag{9}$$

to A_x' mode frequencies $\Omega_\nu[\hat{\mathbf{x}}]$,

$$|S_{\mu x}| \approx \frac{|M_{\mu x}|}{\sqrt{\epsilon(\hat{\mathbf{x}},\infty)}} = \sqrt{\frac{\Pi_\nu(\Omega_\nu^2[\hat{\mathbf{x}}] - \Omega_\mu^2[\mathrm{TO}])}{\Pi_{\nu\neq\mu}(\Omega_\nu^2[\mathrm{TO}] - \Omega_\mu^2[\mathrm{TO}])}}, \tag{10}$$

and to A_z' mode frequencies $\Omega_\nu[\hat{\mathbf{z}}]$,

$$|S_{\mu z}| \approx \frac{|M_{\mu x}|}{\sqrt{\epsilon(\hat{\mathbf{z}},\infty)}} = \sqrt{\frac{\Pi_\nu(\Omega_\nu^2[\hat{\mathbf{z}}] - \Omega_\mu^2[\mathrm{TO}])}{\Pi_{\nu\neq\mu}(\Omega_\nu^2[\mathrm{TO}] - \Omega_\mu^2[\mathrm{TO}])}}, \tag{11}$$

one can obtain absolute values of all nonzero components of $\mathbf{S}_\mu$. (In fact, frequencies of three of the A' modes ($\Omega_7[\hat{\mathbf{x}}], \Omega_{14}[\hat{\mathbf{x}}]$, and $\Omega_{22}[\hat{\mathbf{z}}]$) were shifted by 0.01 cm^{-1} to avoid divergence in the above equations.)

It remains then to figure out the sign s_μ of the $S_{\mu,x}/S_{\mu,z}$ ratio for A_{TO}' modes. This can be done by inspection of the extremal points in the $\mathbf{q}\perp\mathbf{y}$ dispersion. First, one has to locate those extremal points on the A' dispersion curves that correspond to the already known frequencies of A_{TO}' modes. They are shown in Figs. 3, 5, and 7. Obviously, the TO extrema mark directions perpendicular to the corresponding dipoles $\mathbf{d}_\mu = e_\mu^* \mathbf{u}_\mu \| \mathbf{S}_\mu$. The sign s_μ of $S_{\mu,x}/S_{\mu,z}$ is positive if the pair of the inversion related A_{TO}' extremal points falls in even quadrants, and negative in the opposite case. The absolute values of $\mathbf{S}_\mu$ and, for the A' modes, also the angles φ_μ between $\mathbf{S}_\mu$ and $\mathbf{x}$ are given in Tables II and III.

It is interesting to note that a vast majority of $\mathbf{S}_\mu$ vectors for the A' modes actually falls quite close either to the $\mathbf{x}$ or $\mathbf{z}$ directions. For example, the A_{TO}' modes with $\mu = 1,4,10,11,13,21,22,23$ can be considered as $\mathbf{x}$ polarized, and the A_{TO}' modes with $\mu = 3,7,12,14,19,24,27,28$ are clearly $\mathbf{z}$ polarized. It can be taken as support for the ''pseudo-orthorhombic'' definition of the unit cell with a monoclinic angle β of almost 90°, used widely in previous papers and adopted here.

Finally, the frequencies of oblique modes in an arbitrary direction can be calculated from Eqs. (8)–(11) using the values given in Tables II and III. Results of such calculations are shown by continuous lines in Figs. 3, 5, and 7. There are ordinary branches (TO-LO) with minima at a TO frequency and maxima at a LO frequency, but there are also branches with an inverse order (LO-TO) as well as TO-TO [e.g., the $\Omega_1[\mathrm{TO}] - \Omega_2[\mathrm{TO}]$ A' branch in Fig. 3(a)] and LO-LO branches [e.g., the highest-frequency A' branch in Fig. 3(a)]. The existence of such branches together with the characteristic shape of the dispersion curves points to the underlying anticrossings of ''bare'' branches with a more standard angular dispersion.

V. DISCUSSION AND CONCLUSION

In the present study, undertaken at a temperature of about 15 K, we have not detected any line shape anomalies. The very few asymmetric peaks were identified as unresolved doublets, consistent with the complete mode enumeration given here in Tables II and III.

At the same time, we have observed that intrinsic line shape asymmetry certainly does appear in several lines at temperatures above 100 K. Investigation of the gradual development of that asymmetry, line broadening and line frequency shifts with increasing temperature might be of interest but it is beyond the scope of this study. In fact, it would be particularly useful for elucidating the detailed relation between the phonon modes reported here and those measured at room temperature, for example in the Ref. 20.

On the other hand, there is one available independent measurement of a low-temperature $z(xx)\bar{z}$ spectrum that can be straightforwardly compared with the present data. Figures 5.1. and 5.2 of the Ref. 44 shows 8-9 phonon lines observed between 40 and 90 cm^{-1}. These findings are quite similar to our measurements, and only five of the reported lines can be identified with the expected A' modes ($\mu = 24$–28). The additional shoulders and weak modes shows that the problem of ''polarization leakage'' does not appear in our experiment only. We suspect that the partial depolarization or the partial removal of the Raman selection rules may arise due to an intrinsic bulk or surface property of the $Sn_2P_2S_6$ crystal itself.

In any case, we have shown here that there is an alternative way to assign modes, which does not rely on the usual polarization analysis. As far as the modes of different symmetry species can be distinguished by the direction of their dipolar strength, it is sufficient to record directional dispersions of oblique mode frequencies. In the case of the Pn symmetry crystal, it requires one merely to record directional dispersion for a phonon wave vector in the glide plane and in one other perpendicular plane. This approach, largely and successfully used here could be useful in investigations of other crystals for which the polarization analysis happens to be in doubt. Obviously, the approach is most advantageous for polar monoclinic crystals such as $Sn_2P_2S_6$, since besides the symmetry assignment it allows us also to determine the orientations of dipolar strengths of the phonon modes polarized in the monoclinic mirror plane.

ACKNOWLEDGMENTS

We would like to acknowledge stimulating conversations on this subject with M. B. Smirnov from Institute for Silicate Chemistry at St. Petersburg, with J. Petzelt from Institute of Physics AS CR and with Yu. Vysochanskii, A. Grabar, and M. Maior from Uzhgorod University. We are thankful to the research team of Uzhgorod University for providing the excellent single crystals used in this study. V. Studnička from the Institute of Physics kindly performed an x-ray check of the sample orientation. The work has been supported by the INCO-COPERNICUS Project No. ERB3512PL964434 and by the Grant Agency of the Czech Republic (Postdoc Project No. 202/99/D066).

[1] C.D. Carpentier and R. Nitche, Mater. Res. Bull. **9**, 1097 (1974).
[2] B. Scott, M. Pressprich, R.D. Willet, and D.A. Cleary, J. Solid State Chem. **96**, 294 (1992).
[3] S.W.H. Eijt, R. Currat, J.E. Lorentzo, P. Saint-Gregoire, B. Hennion, and Yu.M. Vysochanskii, Eur. Phys. J. B **5**, 169 (1998).
[4] G.M. Curro, V. Grasso, F. Neri, and L. Silipigni, Nuovo Cimento **D20**, 1163 (1998).
[5] Yu.M. Vysochanskii, V.V. Mitrovcij, A.A. Grabar, S.I. Perechinskii, S.F. Motrja, and J. Kroupa, Ferroelectrics **237**, 193 (2000).
[6] D. Baltrunas, A.A. Grabar, K. Mazeika, and Yu.M. Vysochanskii, J. Phys.: Condens. Matter **11**, 2983 (1999).
[7] V. Samulionis, J. Banys, Yu. Vysochanskii, and A. Grabar, Phys. Status Solidi B **215**, 1151 (1999).
[8] M.M. Maior, Fiz. Tverd. Tela (St. Petersburg) **41**, 1456 (1999) [Phys. Solid State **41**, 1333 (1999)].
[9] V. Samulionis, J. Banys, and Yu. Vysochanskii, Ferroelectrics **224**, 517 (1999).
[10] J. Kroupa, Yi. Tyagur, A.A. Grabar, and Yu.M. Vysochanskii, Ferroelectrics **223**, 421 (1999).
[11] M.M. Maior, Yu.M. Vysochanskii, I.P. Prits, S.B. Molnar, L.A. Seikovskaya, and Yu.V. Slivka, Kristallografiya **35**, 1300 (1990).
[12] D.A. Cleary, R.D. Willet, F. Ghebremichael, and M.G. Kuzyk, Solid State Commun. **88**, 39 (1993).
[13] A.A. Grabar, I.V. Kedyk, M.I. Gurzan, I.M. Stoika, A.A. Molnar, and Yu.M. Vysochanskii, Opt. Commun. **188**, 187 (2001).
[14] M. Weber, F. Rickermann, G. von Bally, A. Shumelyuk, and S. Odoulov, Optik (Stuttgart) **111**, 333 (2000).
[15] M. M. Maior, I. P. Prits, and Yu. M. Vysochanskii, Ferroelectrics (to be published).
[16] A. A. Grabar, M. I. Gurzan, I. V. Kedyk, A. A. Molnar, I. M. Stoika, and Yu. M. Vysochanskii, Ferroelectrics (to be published).
[17] Yu.V. Vysochanskii, M.M. Maior, V.M. Rizak, V.Yu. Slivka, and M. Khoma, Zh. Eksp. Teor. Fiz. **95**, 1355 (1985).
[18] A.V. Gomonnai, A.A. Grabar, Yu.M. Vysochanskii, A.D. Belayev, V.F. Machulin, M.I. Gurzan, and V.Yu. Slivka, Fiz. Tverd. Tela (Leningrad) **23**, 3602 (1981) [Sov. Phys. Solid State **23**, 2093 (1981)].
[19] B. Scott, M. Pressprich, R.D. Willet, and D.A. Cleary, J. Solid State Chem. **96**, 294 (1992).
[20] Yu.M. Vysochanskii, V.Yu. Slivka, Yu.V. Voroshilov, M.I. Gurzan, and D.V. Chepur, Fiz. Tverd. Tela (Leningrad) **21**, 211 (1979) [Sov. Phys. Solid State **21**, 123 (1979)].
[21] G. Dittmar and H. Schaffer, Z. Naturforsch. B **29**, 312 (1974).
[22] R. Becker, W. Brockner, and C. Wibbelmann, Z. Naturforsch. Teil A **38A**, 555 (1983).
[23] V.Yu. Slivka, Yu.M. Vysochanskii, M.I. Gurzan, and D.V. Chepur, Fiz. Tverd. Tela (Leningrad) **21**, 2396 (1979) [Sov. Phys. Solid State **21**, 1378 (1979)].
[24] A.V. Gomonnai, Yu.M. Vysochanskii, and V.Yu. Slivka, Fiz. Tverd. Tela (Leningrad) **24**, 1068 (1982).
[25] A.A. Grabar, Yu.M. Vysochanskii, V.G. Furtsev, V.M. Rizak, and V.Yu. Slivka, Ukr. Fiz. Zh. (Russ. Ed.) **31**, 908 (1986).
[26] Yu.M. Vysochanskii, V.Yu. Slivka, A.P. Buturlakin, M.I. Gurzan, and D.V. Chepur, Fiz. Tverd. Tela (Leningrad) **20**, 90 (1978).
[27] V.Yu. Slivka, Yu.M. Vysochanskii, M.I. Gurzan, and D.V. Chepur, Fiz. Tverd. Tela (Leningrad) **20**, 3530 (1978) [Sov. Phys. Solid State **20**, 2042 (1978)].
[28] A.A. Bokotei, Yu.M. Vysochanskii, V.M. Rizak, V.A. Stephanovich, and M.I. Gurzan, Ukr. Fiz. Zh. (Russ. Ed.) **42**, 55 (1997).
[29] A.V. Gomonnai, Yu.M. Vysochanskii, A.A. Grabar, and V.Yu. Slivka, Fiz. Tverd. Tela (Leningrad) **23**, 3623 (1981) [Sov. Phys. Solid State **23**, 2105 (1981)].
[30] Yu.M. Vysochanskii, V.Yu. Slivka, Yu.V. Voroshilov, M.I. Gurzan, and D.V. Chepur, Fiz. Tverd. Tela (Leningrad) **21**, 2402 (1979).
[31] A.A. Grabar, Yu.M. Vysochanskii, N.N. Melnik, S.I. Subbotin, V.V. Panflinov, and V.Yu. Slivka, Fiz. Tverd. Tela (Leningrad) **26**, 65 (1984).
[32] S. Eijt and M. M. Maior, J. Phys. Chem. Sol. B **60**, 631 (1999).
[33] A.A. Grabar, Yu.M. Vysochanskii, and V.Yu. Slivka, Fiz. Tverd. Tela (Leningrad) **26**, 3086 (1984).
[34] V.M. Rizak, A.A. Grabar, Yu.M. Vysochanskii, and V.Yu. Slivka, Fiz. Tverd. Tela (Leningrad) **31**, 154 (1989).
[35] M.B. Smirnov, J. Hlinka, and A. Solov'ev, Phys. Rev. B **61**, 15051 (2000).
[36] H. Burger and H. Falius, Z. Anorg. Allg. Chem. **363**, 24 (1968).
[37] R. Becker and W. Brockner, Z. Naturforsch. Teil A **38A**, 874 (1983).
[38] R. Mercier, J.P. Malugani, B. Fahys, J. Dougade, and G. Robert, J. Solid State Chem. **43**, 151 (1982).
[39] J. Onstott and G. Lucovsky, J. Phys. Chem. Solids **31**, 2171 (1970).
[40] D.J. Olechna, J. Phys. Chem. Solids **31**, 2755 (1970).
[41] L. Merten and G. Lamprecht, Phys. Status Solidi B **39**, 573 (1970).
[42] S.M. Shapiro and J.D. Axe, Phys. Rev. B **6**, 2420 (1972).
[43] Yu. M. Vysochanskii (private communication).
[44] S. Eijt, Ph.D. thesis, University of Nijmegen, 1997.